2019

Volcanic Glass as a Proxy for Cenozoic Elevation and Climate in the Cascade Mountains, Oregon, USA

John Bershaw
Portland State University, bershaw@pdx.edu

Elizabeth J. Cassell
University of Idaho

Tessa Boe Carlson
Portland State University, tessaboe@gmail.com

Ashley R. Streig
Portland State University, streig@pdx.edu

Martin J. Streck
Portland State University, streckm@pdx.edu

Citation Details

Bershaw, J. (2019). Volcanic Glass as a Proxy for Cenozoic Elevation and Climate in the Cascade Mountains. Journal of Volcanology and Geothermal Research, Journal of volcanology and geothermal research , 2019.

Journal of Volcanology and Geothermal Research 381 (2019) 157–167

Contents lists available at ScienceDirect

Journal of Volcanology and Geothermal Research

journal homepage: www.elsevier.com/locate/jvolgeores

Volcanic glass as a proxy for Cenozoic elevation and climate in the Cascade Mountains, Oregon, USA

John Bershaw [a,*], Elizabeth J. Cassel [b], Tessa B. Carlson [a], Ashley R. Streig [a], Martin J. Streck [a]

[a] Portland State University, Portland, OR 97201, USA
[b] University of Idaho, Moscow, ID 83844, USA

ARTICLE INFO

Article history:
Received 19 November 2018
Received in revised form 29 May 2019
Accepted 29 May 2019
Available online 4 June 2019

Keywords:
Volcanic glass
Ash fall tuff
Ignimbrite
Paleoaltimetry
Paleoclimate
Stable isotopes
Pacific Northwest
Cascades

ABSTRACT

After deposition, volcanic glass hydrates with ambient water, recording the average hydrogen isotope ratio (δD or δ^2H) of local meteoric water during the hydration period. Previous researchers have used ancient glass δD values to reconstruct paleotopography and paleoclimate, while others have questioned the long-term reliability of the proxy as a recorder of ancient meteoric water. In this study, we sampled volcanic glasses ranging in age ~33 Ma to <50 ka from tuffs on the leeward (east) side of the Oregon Cascade Mountains. Our results strongly suggest that volcanic glass acquires and preserves δD values that are proportional to the stable isotopic composition of environmental water at the time of ash deposition based on 1) a 20‰ difference in δD values between samples of different ages (~8 Ma apart) from the same locality, 2) preservation of stable isotopic compositions consistent with lacustrine and non-lacustrine depositional environments in coeval samples, and 3) substantial differences between δD values of ancient volcanic glass (>1 Ma) and local meteoric water (converted to glass δD values) throughout the study area.

We propose a paleoenvironmental interpretation of volcanic glass results that resolves previously published isotopic data and agrees well with the petrologic, structural, and stratigraphic record. Namely, the Oregon Cascades have been a significant topographic barrier since at least the mid-Miocene, and likely as far back as the Oligocene. Since reaching a topographic maximum during the eruption of Columbia River flood basalts in the mid-Miocene, surface elevations in Oregon have decreased, while the northern Cascades in Washington continue to rise.

1. Introduction

Hydrogen and oxygen isotope ratios from paleowater, derived from various proxies, can elucidate changes in climate and elevation through time (e.g. Garzione et al., 2000; Poage and Chamberlain, 2001; Kohn and Cerling, 2002; Takeuchi and Larson, 2005; Bershaw et al., 2010; Canavan et al., 2014; Saylor and Horton, 2014; Cassel et al., 2018). Environmental water δD values, preserved within hydrated volcanic glass, have great paleoenvironmental potential, largely due to their widespread deposition and the relatively long timescale of hydration in comparison to other stable isotope proxies (e.g. Cerling and Quade, 1993). Tuffaceous volcanic rocks also typically have dateable phenocrysts and can be spatially correlated based on glass trace element compositions (Sarna-Wojcicki, 1984; Cassel et al., 2012; Cassel and Breecker, 2017). Volcanic glass shards hydrate readily when exposed to environmental water, adding up to 10 wt% water. Recent studies have focused on sample preparation methods and the timescales of preservation to effectively isolate original environmental hydration water δD values (Dettinger and Quade, 2014; Cassel and Breecker, 2017), because, like most paleowater proxies, diagenetic alteration and sample impurities can alter analytical results (Anovitz et al., 2009; Nolan and Bindeman, 2013).

Volcanic glass as a paleowater proxy has been applied across much of western North America (Fig. 1) (e.g. Friedman et al., 1993b; Mulch et al., 2008; Cassel et al., 2009, 2014; Fan et al., 2014; Cassel et al., 2018), but studies that utilize ancient volcanic glass (>1 Ma) have yet to be published in the Pacific Northwest. Here we present the first constraints on paleowater δD values in Oregon from volcanic glasses with ages ranging from ~33 Ma to <50 ka. Samples from the lee (east) side of the Cascade Range provide a record of regional surface elevation and paleoclimate that we interpret within the context of previously published research. Volcanic glass δD values from central Oregon are lower than modern water (converted to glass δD) from early Oligocene to mid-Miocene time, after which δD values increase significantly to present. We suggest that the Oregon Cascades have been a significant topographic barrier since the early Oligocene, and that surface elevations in Oregon decreased after eruption of Columbia River flood basalts (CRBs) in the mid-Miocene, consistent with a tectonic reorganization that reduced subduction-related arc volcanism and initiated rifting in Oregon at that time.

* Corresponding author.
E-mail address: jbershaw@gmail.com (J. Bershaw).

https://doi.org/10.1016/j.jvolgeores.2019.05.021

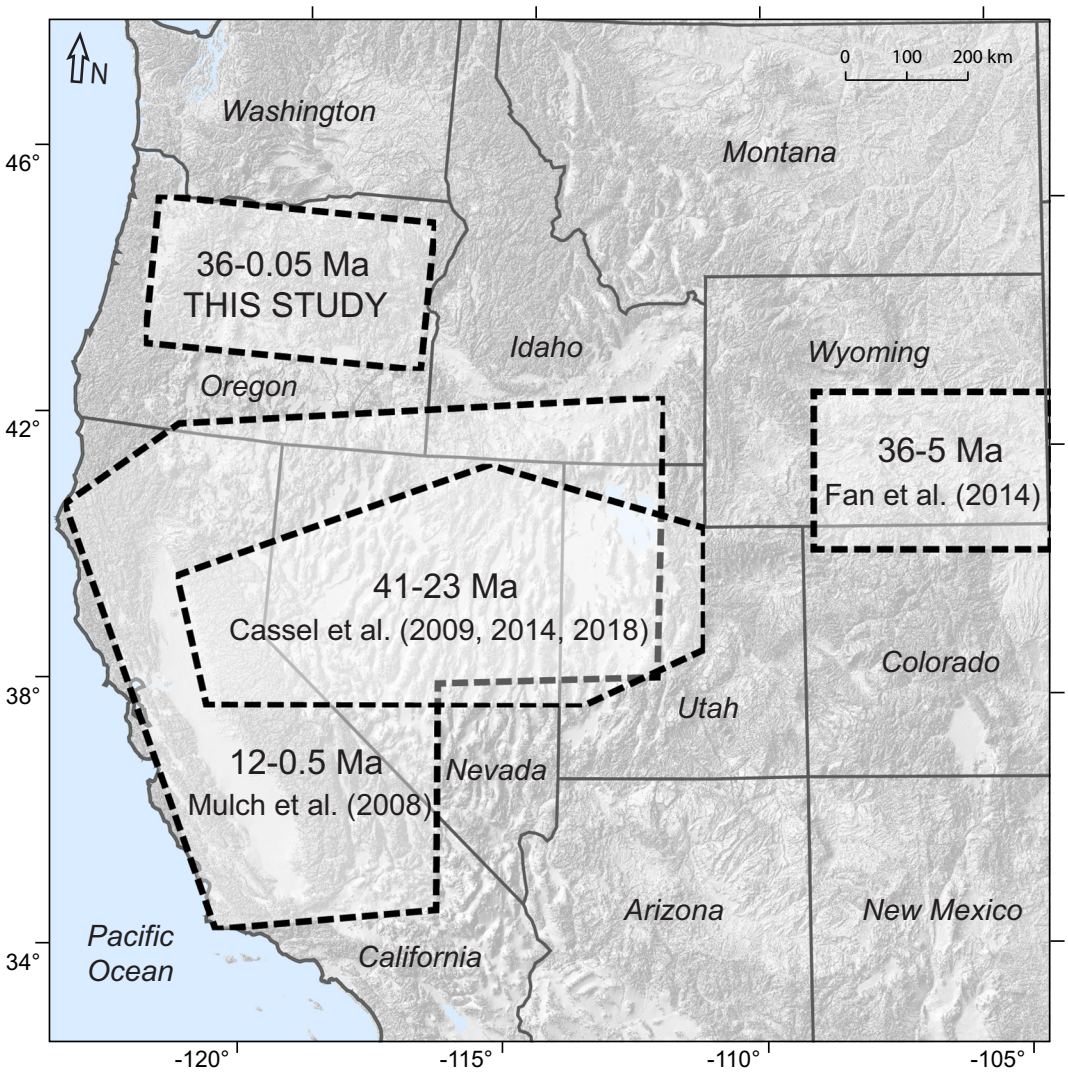

Fig. 1. Hillshade map of the western United States with area of this study labeled. Locations of other volcanic glass paleowater proxy studies >10 ka are shown (Mulch et al., 2008; Cassel et al., 2009, 2014; Fan et al., 2014; Cassel et al., 2018).

2. Background

2.1. Topographic history of the Pacific Northwest

In this study, we focus on the lee (east) side of the Cascade Mountains in central Oregon, characterized as a semi-arid plateau, averaging ~1 km in elevation today (Fig. 2). Central Oregon lies in the rain shadow of the High Cascade Range which strikes roughly north-south and averages ~1.5 km in elevation in Oregon (Fig. 3). Further west is the Coast Range, which is subparallel to the Cascades and averages ~500 m in elevation in Oregon. Cenozoic topography throughout the Pacific Northwest has varied significantly in both space and time. Central Oregon was at sea-level in the mid-Cretaceous (~100 Ma) based on the presence of marine sedimentary rocks (Kleinhans et al., 1984). Subduction-related volcanic and non-marine volcaniclastic rocks of the Clarno Formation erupted in central Oregon starting at ~54 Ma (Vance, 1988; Bestland et al., 1999), and provide the first Cenozoic evidence for extensive subaerial relief. Fossils, paleosols, and sedimentary lithofacies in the Clarno Formation suggest that both tropical lowlands and temperate highlands existed at this time (Retallack, 1991; Bestland et al., 2002).

Subduction moved westward following accretion of the oceanic basaltic Siletzia terrane to North America at about 50 Ma (Snavely Jr and Wells, 1996; Wells et al., 2014). Volcanism shifted west from central Oregon to the modern Cascade arc at ~44 Ma (Snavely Jr and Wells, 1996; Bestland et al., 2002), resulting from subduction of the Juan de Fuca plate beneath North America. By ~35 Ma, the Cascades Range was established from northern California to present-day Mount Rainier (Priest, 1990). Thick accumulations of ignimbrites and ash layers in the John Day Formation in central Oregon, which spans from the Eocene to early Miocene (~39–18 Ma), are evidence of extensive volcanism in the early Cascades (Robinson et al., 1984). Relative to the Quaternary, large eruption volumes from the arc during the Eocene to early Miocene coincide with high plate convergence rates (Verplanck and Duncan, 1987). Volcanic rocks interfinger with thick packages of arc-derived marine sedimentary rocks on the west side of the Cascades during this time, suggesting the Coast Range had not yet developed (Niem et al., 1985; Niem et al., 1992; Retallack et al., 2004a). The emergence of a continuous, subaerial Coast Range in the early Miocene (~20 Ma) pushed marine deposition westward to its modern location (Snavely Jr and Wells, 1996). Compared to the Olympic Mountains in Washington, the Coast Range in Oregon is relatively low in elevation, possibly because of reduced coupling between Siletzia and subducting oceanic crust (Bodmer et al., 2018). Fossils and paleosols from the John Day Formation in central Oregon indicate progressively drier and more open conditions in wooded grasslands by the early Miocene, influenced by global climate change and a developing rain shadow (Retallack, 1991; Retallack, 2004).

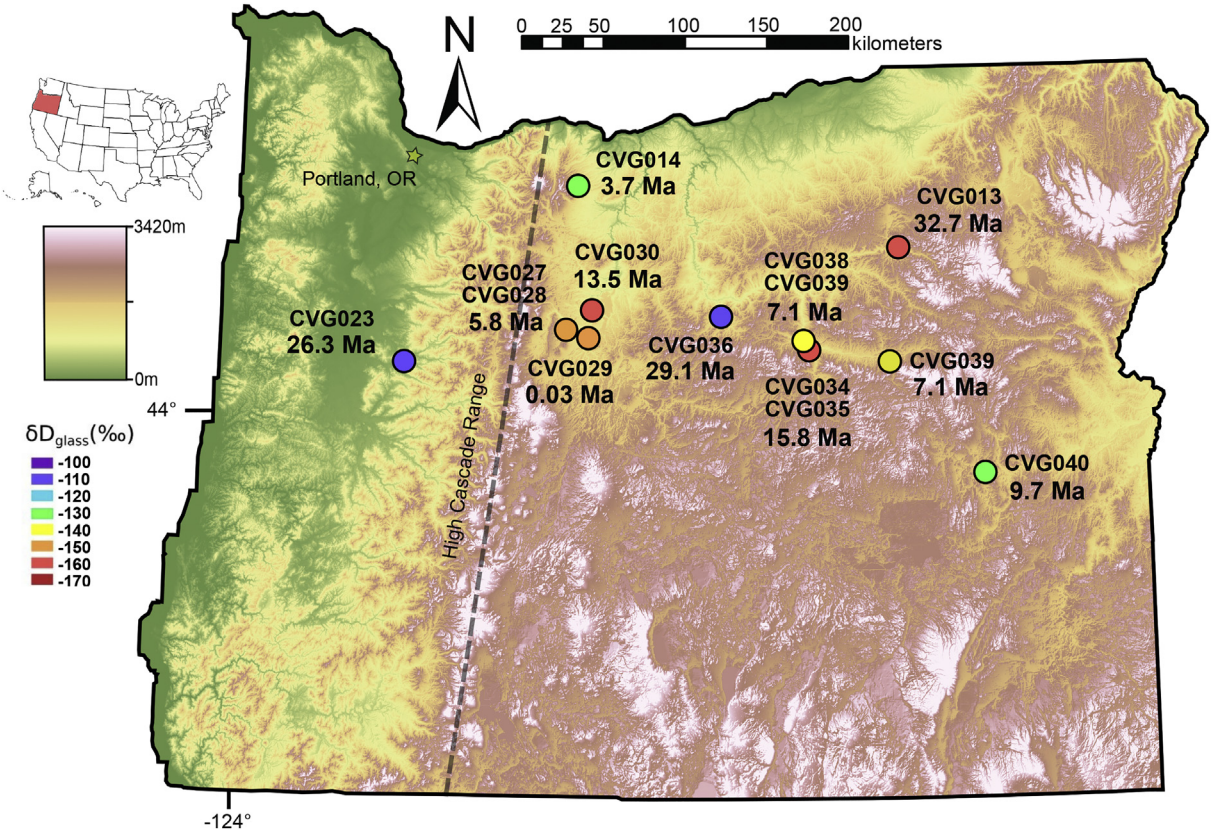

Fig. 2. Digital Elevation Map (DEM) of Oregon showing topography and localities for volcanic glass samples analyzed in this study. Circle color indicates δD values (‰ relative to VSMOW) binned by 10‰ increments. The gray dashed line shows the general trend of the Cascade Mountains.

Volcanism in the Cascade arc remained voluminous until the mid-Miocene, when it waned significantly, possibly due to a slowing of the convergence rate between the North American and Farallon plates (Verplanck and Duncan, 1987; Priest, 1990; Taylor, 1990; Conrey et al., 1997). Beginning ~16.7 Ma, Columbia River flood basalts (CRBs) inundated Oregon and Washington, reaching a thickness of >4 km east of the Cascades (Beeson et al., 1989; Barry et al., 2013; Reidel et al., 2013). At this time, the Cascade arc was relatively quiet, with minimal activity until ~7 Ma (Priest, 1990; Smith, 1993), when lavas, ignimbrites, and volcaniclastics of the Deschutes and Rattlesnake Formations were deposited in central Oregon (Smith et al., 1987; Streck and Grunder, 1995; Pitcher et al., 2017). Fossils and paleosols from these late Miocene units are interpreted to represent a semi-arid, cool climate, similar to that found in central Oregon today (Retallack, 1991; Retallack et al., 2002).

In addition to reduced arc volcanism, the middle to late Miocene marked the initiation of rifting in the Cascade arc, starting in southern Oregon and propagating northward along the arc at ~40 km/Ma

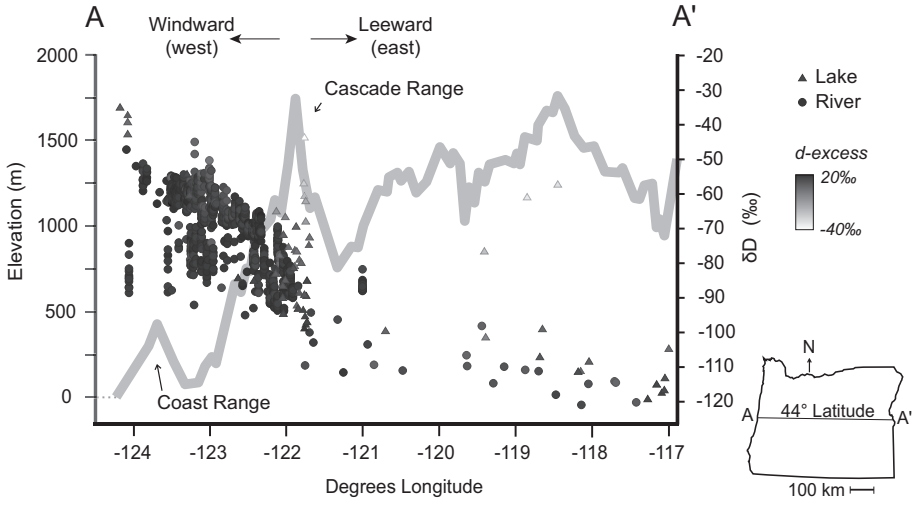

Fig. 3. Hydrogen isotope (δD) values from modern rivers (circles) and lakes (triangles) across Oregon between 42.5° and 45.5° latitude (Supplementary Table S2). The average elevation along a 50 km swath centered at 44° latitude is shown for reference (gray curve). Symbols are shaded by their deuterium excess (d-excess) values showing significant evaporative enrichment in modern lake water (low d-excess, high δD).

(Guffanti and Weaver, 1988; Conrey et al., 1997). Low potassium tholeiites (mid-ocean ridge-like basalts) erupted from the arc during rifting and extend into southern Washington, marking the northern extent of rifting. Elevated hydrothermal heat discharge in the Oregon Cascades is attributed to rifting (Ingebritsen and Mariner, 2010). Data from geothermal exploration wells suggest extension in the Oregon Cascades has resulted in subsidence of ~1 to 3 km from north to south (Conrey et al., 2002). Miocene-Pliocene rifting in the Oregon Cascades is likely related to the clockwise rotation of the Oregon and Washington forearc relative to North America and Basin and Range extension on its trailing edge (Wells and Heller, 1988; Wells and McCaffrey, 2013). While rotation has resulted in extension and subsidence in the Oregon Cascades, the northward component of motion has caused compression in Washington, as it collides with relatively stable Canadian basement (Wells and McCaffrey, 2013). This is demonstrated by the east-west striking Seattle reverse fault which initiated ~13.3 Ma (Brink et al., 2002), north-south shortening in the Yakima fold and thrust belt since ~15 Ma (McCaffrey et al., 2016), and accelerated rock uplift rates in the Washington Cascades during the late Miocene (Reiners et al., 2002). Our volcanic glass results from central Oregon provide a record of regional surface elevation and paleoclimate that we interpret within this geologic context.

2.2. Meteoric water as a proxy for topography and climate

Pacific Northwest climate is controlled by topography and its mid-latitude location in the northern hemisphere where westerlies dominate (Smith et al., 2005). The climate is characterized as Mediterranean in that winters are wet and summers are dry. In the wet season, moist southwesterly air cools overland and encounters orographic barriers (the Coast Range and Cascade Mountains), resulting in steady precipitation (Roe, 2005). There is a stark contrast in precipitation amount across the region exemplified by the Hoh rain forest on the west side of the Olympic Mountains (Washington) which receives up to 400 cm annually, and Richland, a town located in the rain shadow (east) of the Cascades, which receives <20 cm of precipitation (Whiteman, 2000). By summer, the polar jet stream shifts northward and high-pressure cells associated with the subtropical horse latitudes develop over the north Pacific and continental interior, resulting in persistently dry conditions from late June into September. Patterns of atmospheric circulation in the Pacific Northwest have not changed drastically through the Cenozoic, as inferred from depositional patterns of air-fall tuffs in the John Day Formation of central Oregon (Robinson et al., 1990).

Stable isotopes of meteoric water ($\delta^{18}O$ and δD) may be used to estimate surface elevation in regions where precipitation conforms to a simple model of Rayleigh distillation (Rowley and Garzione, 2007). This relationship for δD is observed on the windward (west) side of the Cascade Mountains (−20.3‰/km) (Fig. 3) and is similar to global averages (−22.4‰/km) (Poage and Chamberlain, 2001; Brooks et al., 2012). The relationship between isotopic composition and elevation is complicated by subcloud and surface water evaporation east of the Cascades. Evaporation under low relative humidities increases $\delta^{18}O$ and δD values of the residual meteoric water (Gat, 1996), which can obscure the relationship between the isotopic composition of meteoric water and elevation (Kurita and Yamada, 2008; Bershaw et al., 2016). Many studies have used modern or Rayleigh modeled isotope-elevation relationships (isotopic lapse rates) with a range of temperature and humidity inputs to constrain temporal changes in elevation. These are based on the isotopic composition of ancient water, inferred from proxies in the rock record such as paleosol carbonates, mammal teeth, volcanic glass, lipid biomarkers, and select clays (e.g. Garzione et al., 2000; Mulch et al., 2006; Wang et al., 2008; Kent-Corson et al., 2009; Bershaw et al., 2010; Leier et al., 2013; Cassel et al., 2014; Saylor and Horton, 2014; Kar et al., 2016). A material can be used as a paleoenvironmental proxy if, 1) it is hydrated by meteoric water at or near the time of deposition, 2) isotope fractionation between water and the proxy material is predictable, and 3) the proxy material resists further isotope exchange or diagenetic alteration. Each paleoaltimeter may reflect different types of meteoric water and integrate over different time scales (Rowley and Garzione, 2007).

2.3. Hydration of glass by environmental waters

Ross and Smith (1955) suggested that volcanic glass incorporates and preserves environmental water soon after deposition and Friedman et al. (1993b) showed that volcanic glass preserves its hydrogen isotope composition over geologic timescales. In contact with a glass surface, ambient water will hydrate the glass via the removal and replacement of large-radius ion sites within the glass with H+ and D ions and diffusion through glass pores (Cailleteau et al., 2008; Casey, 2008; Valle et al., 2010; Cassel and Breecker, 2017). The rate of hydration exponentially decreases with time, suggesting that the hydrogen isotope composition of hydrated volcanic glass is largely determined by early exposure to meteoric waters (Friedman et al., 1993b; Nolan and Bindeman, 2013; Gin et al., 2018). It has been shown that volcanic glass hydration rates are not significantly affected by climate (Seligman et al., 2016). Within 10 ka, a silica-rich and insoluble oxide-depleted "gel layer" or "passivating layer" forms on the outermost surface of glass shards due to the reorganization of silica bonds and release of soluble elements via corrosion (Gin et al., 2015). Upon the formation of this layer, the diffusion rate decreases by 3–10 orders of magnitude and can continue to decrease over time (Techer et al., 2001; Valle et al., 2010; Gin et al., 2018).

When volcanic glass hydrates, hydrogen isotopes fractionate so that less deuterium (D or ^2H) is incorporated into the amorphous glass structure relative to protium (^1H), causing a roughly −30‰ shift in the δD value of glass relative to hydrating meteoric waters. This fractionation is empirically defined by Friedman et al. (1993a) using 7 Ma glass spheres from Idaho and a 20 ka ash from New Zealand:

$$\delta D_{environmental\ water} = \frac{(1000 + \delta D_{glass})}{0.967} - 1000 \quad (1)$$

The fractionation factor in Eq. (1) assumes surface temperature and pressure, as ash takes 10^3–10^4 years to reach full hydration (Friedman et al., 1966; Cassel and Breecker, 2017).

2.4. Magmatic water

Prior to hydration by environmental water at the time of quenching, ash contains ~0.1–0.6% magmatic water (Smith, 1960a, 1960b; Friedman et al., 1993b). Though the range in magmatic water δD values is large (Kyser and O'Neil, 1984; Harford and Sparks, 2001), it is likely to have higher δD values than meteoric water in the lee of the Cascade Mountains, as the latter is relatively negative (<−90‰) (Fig. 3). The isotopic composition of water in large glass shards with low water contents (<1 wt% water) can have relatively high δD values (>−70‰), which Seligman et al. (2016) interpret to reflect a mix of magmatic and meteoric water. Studies have estimated the relative contribution of meteoric relative to residual magmatic water in samples using non-hydrated glass δD values (Seligman et al., 2016) or numerical models and thermogravimetry (Giachetti and Gonnermann, 2013; Giachetti et al., 2015; Martin et al., 2017). To minimize magmatic influence, we focus on samples with >2 wt% water (e.g. Friedman et al., 1993b; Fan et al., 2014) and small glass shard sizes (<150 μm) that are more likely to be fully hydrated with meteoric water based on hydration rate measurements (Cassel and Breecker, 2017).

2.5. Post-hydration alteration of δD values

Volcanic glass δD values may be altered long after secondary hydration by environmental water due to a number of factors. Amorphous

glass is thermodynamically unstable compared to mineral phases and is prone to aqueous corrosion including dissolution, alteration, and secondary mineral formation, particularly at elevated temperatures (Sheppard and Gude, 1968; Casey, 2008). Alteration is dependent on environmental conditions such as the temperature and composition of pore fluids and glass, and commonly results in clay mineral growth or complete conversion to clay or zeolite minerals. Nolan and Bindeman (2013) report significant (>100‰) changes in the δD values of glass from Mazama ash samples (7.7 ka) exposed to deuterium labeled water (δD > 650‰) at relatively low temperatures (20–70 °C). Cassel and Breecker (2017) also observe a change in δD values of bulk volcanic glass samples immersed in deuterium labeled water with δD > 18 (18,000‰) for one to two years when samples are not acid abraded prior to analysis, and so attribute this to the addition of precipitates at or near the glass surface. These precipitates are often distributed heterogeneously on glass particles, which can cause large variability in measured values of wt% H_2O and δD (Gin et al., 2011; Hellmann et al., 2015; Cassel and Breecker, 2017; Martin et al., 2017).

The potential for post-hydration alteration of δD values raises the question of whether published volcanic glass records that show δD values similar to modern through time are due to re-equilibration with modern water (e.g. Mulch et al., 2008; Canavan et al., 2014). Though this continues to be a concern, there is evidence that the isotopic composition of *syn*-depositional paleowater is being preserved, but often requires careful sample preparation to isolate. For example, volcanic glasses of Eocene age from differing original depositional environments (lacustrine vs. fluvial) exhibit significant differences in δD values of >100‰, despite being exposed to similar post-depositional meteoric waters for millions of years (Cassel et al., 2014; Cassel and Breecker, 2017). Contamination can impact the overall measured δD value, and some precipitates on shard surfaces can hold significantly more water (12–36 wt %) than glass (2–10 wt%). A combination of hydrofluoric (HF) and hydrochloric (HCl) acid abrasion and heavy liquid separation has been suggested as the most effective way to isolate pure glass shards from hydrated minerals and precipitates adhered to glass surfaces (Cassel and Breecker, 2017).

3. Methods

We targeted felsic volcanic ash samples from across Oregon that range in age from ~33 Ma to <50 ka based on published radiometric and stratigraphic ages (Fig. 2 and Table 1). We collected ~0.5–1 kg of vitric material with no visible evidence of weathering from 5 to 10 cm beneath surface exposures. In total, we analyzed 13 samples from 11 units. Additional information on sample localities, descriptions, and age constraints can be found in Supplementary materials Appendix A.

We used sample preparation methods designed to isolate the isotopic composition (δD) of environmental water within 10 ka of deposition. We sieved shards for a specific grain size fraction (70–150 μm) to minimize the influence of magmatic water. Larger shards may have pristine glass in the center with relatively higher δD values, low water content, and lower overall reproducibility, suggestive of a contribution of magmatic water from the center of larger shards (Dettinger and Quade, 2014; Seligman et al., 2016). In addition, large shards may not completely de-gas during TC/EA analysis (Martin et al., 2017). Samples between 70 and 150 μm have also been shown to be more homogeneously hydrated (≥2% water) (Cassel and Breecker, 2017).

We used heavy liquid and magnetic separation to isolate glass shards from other tuff components (e.g. Sarna-Wojcicki, 1984; Mulch et al., 2008; Cassel and Breecker, 2017; Smith et al., 2017). We routinely checked each sample for purity via petrographic analysis and stopped when samples contained ≥99% isotropic glass. Adhering phenocrysts can be problematic for some ashes, including Mazama ash which contains adhered micro-phenocrysts (Seligman et al., 2016). These minerals may have melt inclusions containing magmatic water, which affects glass δD values (Kent, 2008; Moore, 2008; Cassel and Breecker, 2017).

Samples were abraded with 8% HF to remove surface precipitates and altered glass, and to detach adhered phenocrysts. Samples that appeared altered (i.e. exhibited birefringence in cross-polarized light) after two rounds of HF treatment were not analyzed. Whether HF abrasion is necessary for glass δD value analysis is debated, as HF pretreatment in relatively young glass (<1 Ma) has been shown to increase variability between unique samples (Dettinger and Quade, 2014; Seligman et al., 2016), but to decrease inter-replicate variability (Cassel and Breecker, 2017). Older samples (>1 Ma) in these studies do not show evidence of alteration from HF abrasion, regardless of deposition environment. Numerous studies have used HF to reduce the presence of surface precipitates that may form long after ash deposition (e.g. Mulch et al., 2008; Cassel et al., 2014; Fan et al., 2014; Pingel et al., 2014; Rohrmann et al., 2016; Smith et al., 2017).

Samples were analyzed at the Light Stable Isotope Lab at the University of Texas at Austin on a TC/EA coupled to a MAT-253 IRMS following Cassel and Breecker (2017). Reported wt% water and δD values are the averages of two analyses (one replicate) (Table 1). Age ranges include 2σ uncertainty based on radiometric dates or relative dating based on stratigraphic context. International standard δD values were reproducible within ±3‰ (2σ). Detailed descriptions of sample preparation and analytical methods are included in Supplementary materials Appendices B and C.

4. Results

4.1. Volcanic glass water content

The average inter-replicate range in water content for samples is 0.12% (Table 1). The water content in samples averages 4.79 wt% (σ = 3.0). The water content within a sample does not show a significant correlation with age ($R^2 = 0.1$) (Fig. 4). Water content does appear to be related to sample texture, with welded samples (excluding sample CVG023 from the windward side of the Cascades) having the least water (average = 2.63 wt%) and non-welded samples containing more water (average = 4.61 wt%) (Table 1).

4.2. Volcanic glass δD values

For all samples, the inter-replicate range in δD values averages 1.7‰. One sample (CVG036) with an exceptionally low wt% water content (1.16%) had an anomalously high range in δD values among replicates (5.4‰). We do not observe a significant correlation between δD value and age ($R^2 < 0.01$) (Fig. 5).

5. Discussion

5.1. Evidence that volcanic glass preserves paleoenvironmental water

If volcanic glass continuously re-equilibrates with meteoric waters, all glass samples exposed to similar modern waters should have similar δD values, regardless of age. However, samples show unit-dependent variation in δD values at one location, consistent with preservation of original meteoric hydration waters and reflecting changes in the δD values of meteoric water over time. Three unwelded samples of different ages were collected within three kilometers of one another and are currently exposed to precipitation with similar δD values, so have access to similar ambient pore waters. Glass in sample CVG038 from the Rattlesnake Tuff (~7 Ma) yields a δD value of −145.5‰. Two glass samples from the underlying Mascall Formation 15.8 Ma), CVG034 and CVG035, have δD values within 2.5‰ of each other: −165.6‰ and −163.3‰, ~20‰ lower than the overlying Rattlesnake tuff. These results suggest that volcanic glass is preserving original paleoenvironmental water δD values from the time of ash deposition,

Table 1
Volcanic glass sample meta-data and results. Refer to Supplementary materials Appendix A for more detail on sample locations and field observations. Ranges in wt% water and δD are based on one replicate for each sample. Age ranges are 2σ uncertainty based on radiometric dates or relative date range based on stratigraphic context.

Name/formation	Sample ID	Lat	Long	Elevation (m)	Depositional environment	Interpreted water	Welding	wt% H_2O	Range wt% H_2O	δD_{glass} (‰)	Range δD_{glass} (‰)	Age (Ma)	Age uncertainty	Age/location reference
Quaternary Ash	CVG029	44.544480	−121.258290	735	Aeolian	Precipitation	Non-welded	3.19	0.19	−151.3	1.1	0.025	0.025	Peterson and Groh, 1970
Tuff of Friend	CVG014	45.362130	−121.341880	874	Pyroclastic Flow	Precipitation	Welded	3.07	0	−134	2.3	3.68	0.02	McClaughry et al., unpublished
Deschutes Formation	CVG027	44.580830	−121.425030	697	Fluvial	Stream	Non-welded	3.95	0.03	−151.8	1.6	5.83	0.16	Pitcher et al., 2017
Deschutes Formation	CVG028	44.581540	−121.428320	676	Fluvial	Stream	Non-welded	4.6	0.06	−149.2	1.1	5.83	0.16	Pitcher et al., 2017
Rattlesnake Tuff	CVG038	44.521213	−119.633427	996	Pyroclastic Flow	Precipitation	Non-welded	2.87	0.08	−145.5	0.9	7.05	0.01	Streck et al., 2004; Streck and Grunder, 1995
Rattlesnake Tuff	CVG039	44.408178	−118.987484	1021	Pyroclastic Flow	Precipitation	Non-welded	2.99	0.05	−143.6	0.9	7.05	0.01	Streck et al., 2004; Streck and Grunder, 1995
Devine Canyon Tuff	CVG040	43.784512	−118.278759	1280	Lacustrine	Lake	Non-welded	4.17	0.43	−132.1	1.4	9.74	0.04	Jordan et al., 2004; Streck et al., 2004; Streck et al., 1999; Greene, 1973
Simtustus Formation	CVG030	44.694780	−121.230000	486	Fluvial	Stream	Non-welded	8.13	0.25	−158.1	1.4	13.5	1.5	Smith, 1985
Dreamtime Tuff	CVG035	44.501390	−119.625000	722	Fluvial	Stream	Non-welded	6.11	0.05	−165.6	1.8	15.77	1.4	Bestland et al., 2008; Fiebelkorn et al., 1982
Kangaroo Tuff	CVG034	44.499720	−119.625280	771	Fluvial	Stream	Non-welded	5.48	0.15	−163.3	1.1	15.77	1.4	Bestland et al., 2008; Fiebelkorn et al., 1982
Tuff of Foster Dam	CVG023	44.419920	−122.665320	205	Pyroclastic Flow	Precipitation	Welded	12.83	0.18	−108.4	2.3	26.28	0.18	McClaughry et al., 2010
Picture Gorge Ignimbrite	CVG036	44.656940	−120.261670	708	Pyroclastic Flow	Magmatic	Welded	1.16	0.05	−112.8	5.4	29.07	0.01	Laib, 2016
Tuff of Dale	CVG013	45.013140	−118.890630	936	Pyroclastic Flow	Precipitation	Welded	3.67	0.04	−155.4	0.2	32.66	0.36	Brown, 2017; Ferns et al., 2001; Savoie, 2013

consistent with other studies (Friedman et al., 1993b; Cassel and Breecker, 2017; Smith et al., 2017). Though unlikely, we cannot rule out the possibility that recent groundwater is affecting the Rattlesnake Tuff sample (CVG038) without affecting the Mascall Formation samples (CVG034 and CVG035), resulting in variable δD values within a single outcrop (e.g. Sanyal et al., 2005).

Lakes may exhibit much higher δD values (>100‰) compared to nearby streams and precipitation (Fig. 3), particularly in closed, evaporative basins (Gonfiantini, 1986; Talbot, 1990). The Devine Canyon Tuff sample (CVG040) was collected above a tabular diatomite bed indicative of a lacustrine depositional environment. For this lacustrine sample, the δD value was over 10‰ higher than any other non-welded sample from the rain shadow (east) of the Cascades (solid diamond in Fig. 5), suggesting that its isotopic composition is reflective of its depositional environment relative to other ancient glass samples. Though the sample was not >99% pure glass, low inter-replicate variability (<2‰) suggests that the relatively high δD values are reliable.

Lastly, ancient glass (>1 Ma) has consistently more negative δD values than modern water nearby, suggesting re-equilibration with modern water is not occurring. East of the Cascades (> −122° longitude), modern meteoric water δD values, converted to glass δD values using Eq. (1) are >−145‰ while ancient volcanic glass δD values are <−145‰ (Fig. 6). Recent (<50 ka) volcanic glass δD values generally overlap with modern stream water converted to glass. The exceptions are three samples near the Cascade crest that have more negative δD values than modern water.

5.2. Paleoenvironmental interpretations

We limit our discussion to volcanic glass samples that were hydrated by stream water or precipitation as they are a more accurate proxy for paleoclimate and topography (Table 1). δD values from volcanic glass are averaged within 2 Ma increments to show temporal trends in the context of other paleowater proxies and major tectonic and climatic events (Fig. 7). Starting in the Oligocene, average volcanic glass δD values in central Oregon decrease 9.1‰ from −155.4‰ to a minimum of −164.5‰ in the mid-Miocene. Volcanic glass δD values progressively increase from the mid-Miocene to present by 34.6‰. This is the difference between mid-Miocene (15.8 Ma) and recent volcanic glass (7.7–<50 ka), the latter of which averages −129.9‰ and is largely based on Mazama ash samples published in Seligman et al. (2016) (Supplementary Table S1). Though the range in recent volcanic glass δD values is large (1σ standard deviation of 13.4‰), they are consistent with modern water converted to glass (Figs. 5 and 7). Prior to considering changes in δD values related to local climate and surface elevations, we assess the impact of global climate change on these trends.

Changes in temperature at the oceanic source of vapor impact the isotopic composition of meteoric water downwind (Rozanski et al., 1993). However, sea-surface temperatures at mid-latitudes (~45°) in the Northern Hemisphere have not shifted significantly through the Cenozoic relative to the Holocene (Zachos et al., 1994). That said, the isotopic composition of the ocean, from which most Pacific Northwest moisture is derived, has evolved through the Cenozoic due to changes in polar ice-volumes (Zachos et al., 2001). An ice sheet became established over Antarctica sometime in the late Eocene (Fig. 7). Partial melting of the ice-sheet in the late Oligocene led to a decrease in ocean $\delta^{18}O$ of ~0.7‰ (δD ~5.5‰ = $\delta^{18}O * 8$) (Zachos et al., 2001). This may explain over half of the modest 9‰ decrease we observe in volcanic glass from Oligocene to mid-Miocene time. After the mid-Miocene Climatic Optimum, ice-sheets became established at both poles by the mid-Pliocene, increasing ocean $\delta^{18}O$ by ~2‰ (δD ~16‰ = $\delta^{18}O * 8$). This could account for less than half of the 34.6‰ increase in δD that we observe from the mid-Miocene to present, leaving an increase of 18.6‰ (± 13.4‰) that is related to regional topography and local climate change. Uncertainty is based on the 1σ standard deviation in recent (7.7 ka)

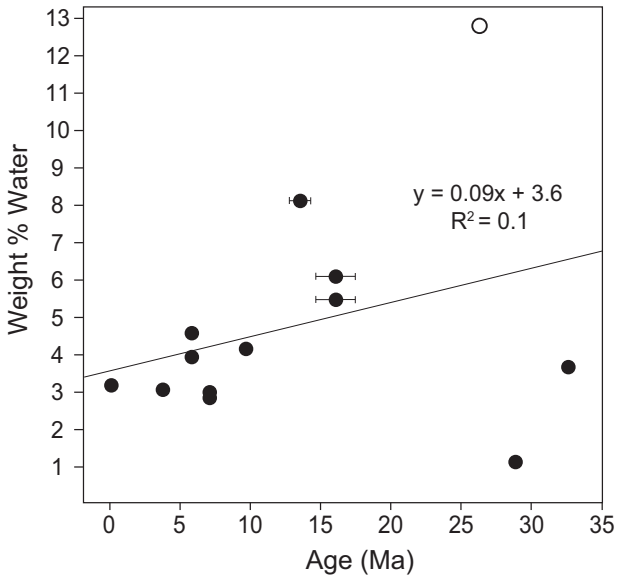

Fig. 4. Average water content (weight %) versus Age (Ma) for all analyzed samples. The open circle is the Tuff of Foster Dam (CVG023), the only sample taken from the windward (west) side of the Cascade Mountains. There is not a significant correlation ($R^2 = 0.1$). Error bars have been removed when smaller than the symbol.

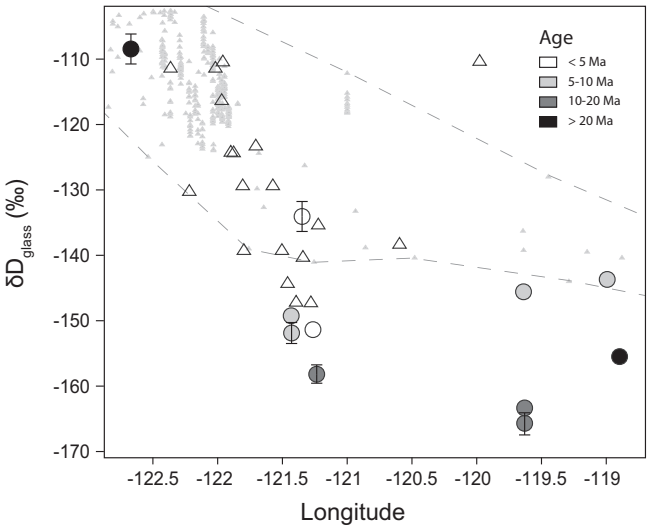

Fig. 6. The isotopic composition of volcanic glass (δD) from samples that have >2 wt% water (non-magmatic) and are interpreted to be hydrated by streams or precipitation. Symbols are colored by age (dark is old, light is young) with error bars that represent δD uncertainty. Mazama ash samples (~7.7 ka) are shown as open triangles and are from Seligman et al. (2016). Modern river δD values converted to glass using Eq. (1) (Friedman et al., 1993a) are shown as small triangles with their envelope defined by the dashed lines (Supplementary Table S2). The Cascades are at about −122° longitude. Most ancient (>1 Ma) volcanic glass samples have more negative δD values than recent ash (open symbols) and modern water nearby.

volcanic glass published in Seligman et al. (2016) and our single Quaternary ash sample (Fig. 5).

An increase in δD values since the mid-Miocene could be interpreted as aridification in a developing Cascade Range rain shadow. Higher aridity during the late Miocene and Pliocene would likely cause subcloud evaporation of raindrops and evaporative enrichment of surface waters as observed in many lee sides of mountain ranges (Kent-Corson et al., 2009; Saylor et al., 2009; Caves et al., 2015; Bershaw et al., 2016). This is the interpretation proposed by previous workers who conclude that the Cascade Mountains have increased in surface elevation since the mid-Miocene (Kohn et al., 2002; Takeuchi and Larson, 2005; Kohn and Law, 2006; Takeuchi et al., 2010). In these studies, decreases in $\delta^{18}O$ of paleowater proxy minerals are interpreted as an increase in Cascade Mountain surface elevation while increases in $\delta^{18}O$ are interpreted as aridification in the attendant rain shadow (Fig. 7). This ambiguity demonstrates how paleowater proxy records themselves are often underconstrained, resulting in non-unique solutions or interpretations (e.g. Ehlers and Poulsen, 2009; Galewsky, 2009; Botsyun et al., 2019). Here we propose an alternative interpretation: that an 18.6‰ increase in volcanic glass δD values since the mid-Miocene is due to a *decrease* in surface elevation of the Oregon Cascades over that time, in agreement

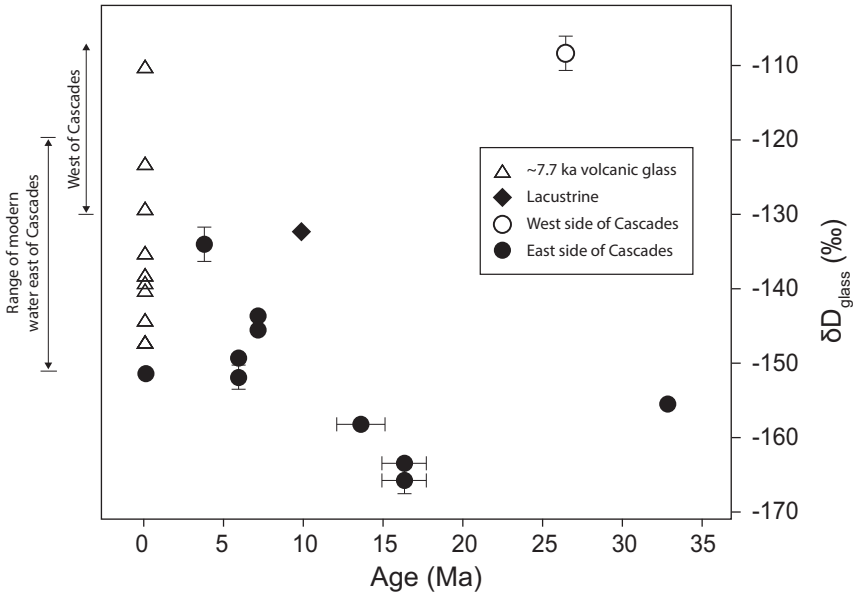

Fig. 5. The isotopic composition of volcanic glass (δD) from samples that have >2 wt% water (non-magmatic). Solid circles are samples collected from the east side (rain shadow) of the Cascade Mountains and the open circle is a sample (CVG023) collected from the west (windward) side. The solid diamond is from a lacustrine sample (CVG040). All others are interpreted to be hydrated by streams or precipitation. Age and δD value do not correlate ($R^2 < 0.01$). However, R^2 goes up to 0.58 when non-lacustrine, middle Miocene and younger samples are considered. Mazama ash samples (~7.7 ka) are shown as open triangles and are from Seligman et al. (2016). The range of modern stream water δD converted to glass using Eq. (1) (Friedman et al., 1993a) on both the west and east sides of the Cascade Mountains are shown to the left of the plot for reference (Supplementary Table S2). Horizontal and vertical error bars represent age and δD uncertainty respectively.

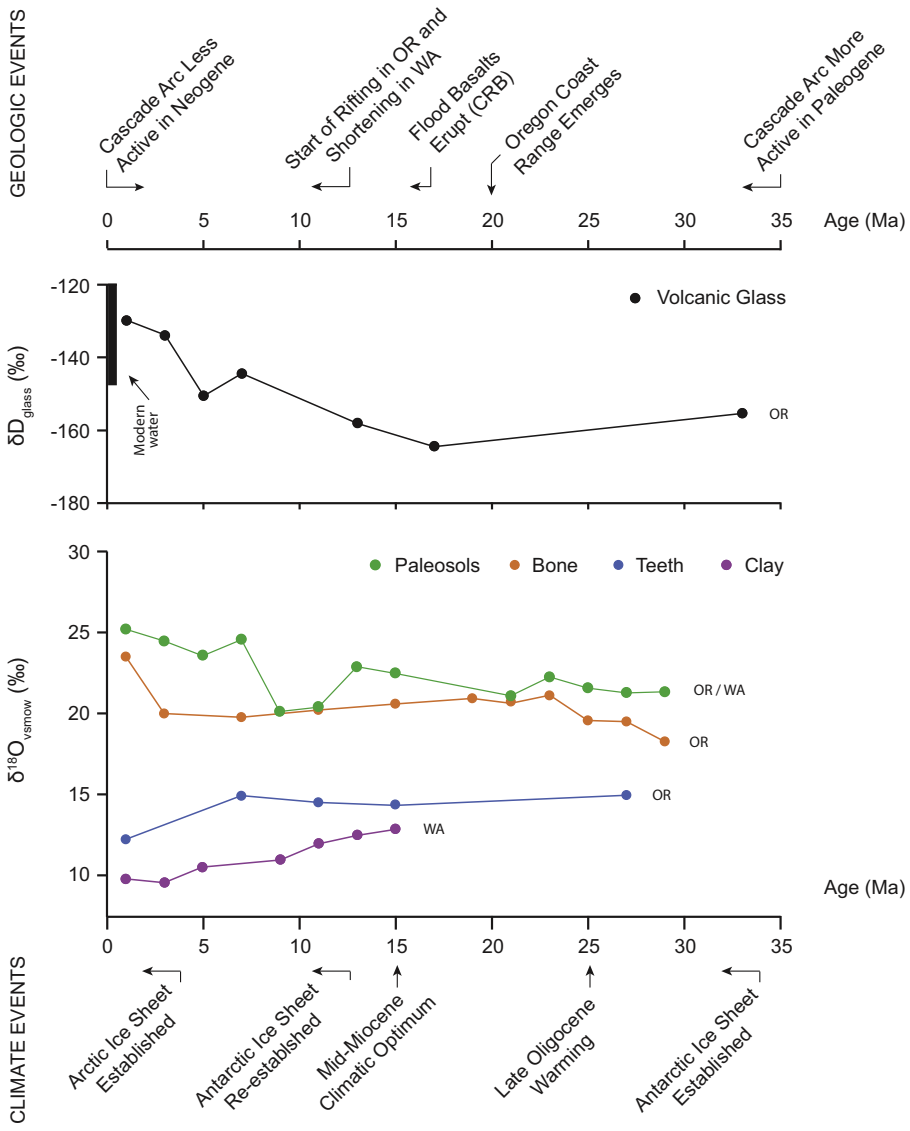

Fig. 7. Comparison of isotopic proxy record data relative to major geologic events in the Pacific Northwest. Each curve connects the average isotopic composition of all samples within 2 Ma bins, i.e. from 0–2 Ma, 2–4 Ma, 4–6 Ma, and so on. The range of volcanic glass δD values is shown in Fig. 5. Recent (~7.7 ka) volcanic glass data is included from Seligman et al. (2016). In the volcanic glass plot, the range of modern stream water δD converted to glass using Eq. (1) (Friedman et al., 1993a) on the east side of the Cascade Mountains is shown as a black rectangle (Supplementary Table S2). Only paleowater proxy samples from Oregon (OR) and Washington (WA) are included. Paleosol data is from Takeuchi et al. (2010), (Retallack et al., 2004b), and (Lechler et al., 2018). Bone data is from Kohn and Law (2006). Tooth data is from Kohn et al. (2002). Clay data is from Takeuchi and Larson (2005). Background Section 2.1 contains references for geologic events. Climatic events are modified from Zachos et al. (2001).

with previously published petrologic, structural, and stratigraphic research on Cascade evolution.

Subsidence following the eruption of the CRBs in the mid-Miocene is consistent with a lull in Cascade volcanism and the development of rifting in the Oregon Cascades (Priest, 1990; Conrey et al., 1997, 2002). Prior to rifting in Oregon, it is plausible that the minimum δD values in the mid-Miocene reflect high topography associated with emergence of the Oregon Coast Range and eruption of the CRBs, which spread out across Oregon and Washington and followed the ancestral Columbia River through the Cascades to the Pacific Ocean. Voluminous flood basalts would have filled topographic lows, reducing low elevation pathways for westerly-derived moisture, causing a decrease in the isotopic composition of meteoric water (e.g. Lechler and Galewsky, 2013). Geophysical evidence shows that regional thermal uplift also peaked at CRB time, when a large volume of hot mantle intruded underneath the Pacific Northwest, followed by subsidence (Zhou and Liu, 2019).

A lowering of surface elevations in Oregon since the mid-Miocene is also consistent with an increase in $\delta^{18}O$ values of paleosol carbonates and bone (Fig. 7). Meanwhile, a ~4‰ decrease in $\delta^{18}O$ from clay samples in central Washington (Takeuchi and Larson, 2005) suggests the Washington Cascades may have increased in surface elevation while the Oregon Cascades were subsiding. In fact, contemporaneous shortening in Washington and extension in Oregon is predicted by the model of Cascade arc rotation described by Wells and McCaffrey (2013). An increase in $\delta^{13}C$ values since the mid-Miocene from paleosol carbonates and bone from central Oregon (not shown) have been interpreted as aridification in an emerging Cascade rain shadow (Kohn and Law, 2006; Takeuchi et al., 2010). However, modeling of atmospheric circulation over mountain ranges suggests there is a threshold elevation over which rain shadow development stops (Galewsky, 2009). Thus, a decrease in elevation of the Cascade Mountains does not require a more temperate climate in the lee, so long as a rain shadow threshold elevation is met. In addition, temperate highlands and semi-arid, grassy lowlands have coexisted in central Oregon since the Oligocene, based on the interpretation of dissimilar climates at the same stratigraphic levels throughout the John Day Formation (Retallack, 1991; Bestland et al.,

1999). Within the Oregon Cascade rain shadow today, more arid conditions exist at lower elevations, which could explain increases in paleosol and bone $\delta^{13}C$ values since the mid-Miocene.

Our oldest volcanic glass data shows that δD values from central Oregon were also relatively low prior to CRB eruption. The largest observed variation in ancient glass δD values is not temporal, but spatial, from the west to east side of the Cascade Mountains. The 26 Ma Tuff of Foster Dam sample (CVG023), collected from the west side of the Cascades, is 47‰ higher than the 32 Ma Tuff of Dale sample (CVG013), collected east of the Cascades (Fig. 5). This suggests that the Cascades have been a topographic barrier since the Oligocene. Late Oligocene paleosols and fossils from the John Day Formation in central Oregon are indicative of a semi-arid climate similar to today, supporting the existence of a rain shadow at that time (Retallack, 2004; Retallack et al., 2004b). Some topography associated with the Cascades magmatic arc likely existed through much of the Cenozoic as subduction has occurred near its current position since ~45 Ma, after the Siletzia Terrane accreted onto North America (Sherrod and Smith, 2000; Schmandt and Humphreys, 2011; Wells et al., 2014). Paleogene igneous rocks and volcaniclastic rocks of the John Day Formation show that an extensive magmatic arc was established from northern California to Mount Rainer in Washington State by the Oligocene (Robinson et al., 1984; Priest, 1990; Bestland et al., 1999).

6. Conclusions

Our results indicate that volcanic glass preserves paleowater δD values, as samples from units of different ages at the same locality yield distinct δD values (20‰ difference) that reflect their original depositional environments, and Oligocene to Miocene volcanic glass δD values in central Oregon are generally lower than recent glass (<50 ka) and modern meteoric water converted to glass. Volcanic glass continues to be a valuable addition to paleowater proxy toolkits but requires an understanding of unit depositional environment and water-glass interaction, from original magmatic water to secondary hydration, as well as strict adherence to sample preparation protocols, for robust estimation of paleowater δD values.

Previous researchers have interpreted trends in paleowater proxies from central Oregon and Washington as an increase in surface elevation of the Cascades since ~15 Ma, resulting in lee side aridification. Alternatively, we suggest the Oregon Cascades have been a major topographic barrier since at least the mid-Miocene, and likely as far back as the Oligocene. After reaching a topographic maximum during the eruption of CRBs, surface elevations in Oregon have decreased, while the northern Cascades in Washington continue to rise. Using the modern isotopic lapse rate observed in the Oregon Cascades of −20.3‰/km (Brooks et al., 2012), an increase in δD values of 18.6‰ ± 13.4 (corrected for changes in global ice volume) equates to a decrease in elevation of 916 m ± 660 m since the mid-Miocene. Uncertainty is based on 1σ standard deviation of recent (<50 ka) volcanic glass. This estimate is consistent with subsidence estimates for the Cascades in northern Oregon (Conrey et al., 2002), but may also be related to CRB denudation and/or regional thermal subsidence (Zhou and Liu, 2019).

Acknowledgements

We would like to thank Andrew Canada, Emily White, Zach Foster-Baril, and Eric Stauffer for assistance with sample preparation, Toti Larson for assistance in sample analysis, and Jiaming Yang for assistance in the field. We would also like to thank Ray Wells, Kenneth Cruikshank, Joel Saylor, and an anonymous reviewer for providing feedback that improved the manuscript substantially. This research is based largely on the Master's Thesis of Tessa Carlson (Carlson, 2018). It was supported by two Geological Society of America (GSA) Student Research Grants to Tessa Carlson.

Appendices. Supplementary data

Supplementary data to this article can be found online at https://doi.org/10.1016/j.jvolgeores.2019.05.021.

References

Anovitz, L.M., Cole, D.R., Riciputi, L.R., 2009. Low-temperature isotopic exchange in obsidian: implications for diffusive mechanisms. Geochim. Cosmochim. Acta 73, 3795–3806.
Barry, T., Kelley, S., Reidel, S., Camp, V., Self, S., Jarboe, N., Duncan, R., Renne, P., Ross, M., Wolff, J., 2013. Eruption chronology of the Columbia River Basalt Group. The Columbia River Flood Basalt Province: Geological Society of America Special Paper 497, 45–66.
Beeson, M.H., Tolan, T., Anderson, J., 1989. The Columbia River Basalt Group in western Oregon; geologic structures and other factors that controlled flow emplacement patterns. In: Reidel, S.P., Hooper, P.R. (Eds.), Volancism and Tectonism in the Colum~ bia River Flood-Basalt Province: Geological Society of America Special Paper. vol. 239, pp. 223–246.
Bershaw, J., Garzione, C.N., Higgins, P., MacFadden, B.J., Anaya, F., Alvarenga, H., 2010. Spatial–temporal changes in Andean plateau climate and elevation from stable isotopes of mammal teeth. Earth Planet. Sci. Lett. 289, 530–538.
Bershaw, J., Saylor, J.E., Garzione, C.N., Leier, A., Sundell, K.E., 2016. Stable isotope variations (δ 18 O and δD) in modern waters across the Andean Plateau. Geochim. Cosmochim. Acta 194, 310–324.
Bestland, E., Hammond, P., Blackwell, D., Kays, M., Retallack, G., Stimac, J., 1999. Geologic framework of the Clarno Unit, John Day Fossil Beds National Monument, central Oregon. Or. Geol. 61, 3–19.
Bestland, E.A., Hammond, P.E., Blackwell, D.L.S., Kays, M.A., Retallack, G.J., Stimac, J., 2002. Geologic framework of the Clarno Unit, John Day Fossil Beds National Monument, Central Oregon. Oregon Department of Geology and Mineral Industries Open-file Report.
Bestland, E.A., Forbes, M.S., Krull, E.S., Retallack, G.J., Fremd, T., 2008. Stratigraphy, paleopedology, and geochemistry of the middle Miocene Mascall Formation (type area, central Oregon, USA). PaleoBios 28, 41–61.
Bodmer, M., Toomey, D.R., Hooft, E.E., Schmandt, B., 2018. Buoyant asthenosphere beneath Cascadia influences megathrust segmentation. Geophys. Res. Lett. 45, 6954–6962.
Botsyun, S., Sepulchre, P., Donnadieu, Y., Risi, C., Licht, A., Rugenstein, J.K.C., 2019. Revised paleoaltimetry data show low Tibetan Plateau elevation during the Eocene. Science 363, eaaq1436.
Brink, U.t., Molzer, P., Fisher, M., Blakely, R., Bucknam, R., Parsons, T., Crosson, R., Creager, K., 2002. Subsurface geometry and evolution of the Seattle fault zone and the Seattle basin, Washington. Bull. Seismol. Soc. Am. 92, 1737–1753.
Brooks, J.R., Wigington, P.J., Phillips, D.L., Comeleo, R., Coulombe, R., 2012. Willamette River Basin surface water isoscape (δ18O and δ2H): temporal changes of source water within the river. Ecosphere 3, art39.
Brown, E.A., 2017. Rhyolite Petrogenesis at Tower Mountain Caldera, OR, Geology. Portland State University.
Cailleteau, C., Angeli, F., Devreux, F., Gin, S., Jestin, J., Jollivet, P., Spalla, O., 2008. Insight into silicate-glass corrosion mechanisms. Nat. Mater. 7, 978–983.
Canavan, R.R., Carrapa, B., Clementz, M.T., Quade, J., DeCelles, P.G., Schoenbohm, L.M., 2014. Early Cenozoic uplift of the Puna Plateau, Central Andes, based on stable isotope paleoaltimetry of hydrated volcanic glass. Geology 42, 447–450.
Carlson, T.B., 2018. Volcanic Glass as a Paleoenvironmental Proxy: Comparing Preparation Methods on Ashes From the Lee of the Cascade Range in Oregon, USA. Portland State University.
Casey, W.H., 2008. Dynamics and durability. Nat. Mater. 7, 930.
Cassel, E.J., Breecker, D.O., 2017. Long-term stability of hydrogen isotope ratios in hydrated volcanic glass. Geochim. Cosmochim. Acta 200, 67–86.
Cassel, E.J., Graham, S.A., Chamberlain, C.P., 2009. Cenozoic tectonic and topographic evolution of the northern Sierra Nevada, California, through stable isotope paleoaltimetry in volcanic glass. Geology 37, 547–550.
Cassel, E.J., Graham, S.A., Chamberlain, C.P., Henry, C.D., 2012. Early Cenozoic topography, morphology, and tectonics of the northern Sierra Nevada and western Basin and Range. Geosphere 8, 229–249.
Cassel, E.J., Breecker, D.O., Henry, C.D., Larson, T.E., Stockli, D.F., 2014. Profile of a paleoorogen: high topography across the present-day basin and range from 40 to 23 Ma. Geology 42, 1007–1010.
Cassel, E.J., Smith, M.E., Jicha, B.R., 2018. The impact of slab rollback on earth's surface: uplift and extension in the hinterland of the North American Cordillera. Geophys. Res. Lett. 45 (20), 10–996.
Caves, J.K., Winnick, M.J., Graham, S.A., Sjostrom, D.J., Mulch, A., Chamberlain, C.P., 2015. Role of the westerlies in Central Asia climate over the Cenozoic. Earth Planet. Sci. Lett. 428, 33–43.
Cerling, T.E., Quade, J., 1993. Stable carbon and oxygen isotopes in soil carbonates. Climate Change in Continental Isotopic Records. vol. 78, pp. 217–231.
Conrey, R.M., Sherrod, D.R., Hooper, P.R., Swanson, D.A., 1997. Diverse primitive magmas in the Cascade arc, northern Oregon and southern Washington. Can. Mineral. 35, 367–396.
Conrey, R.M., Taylor, E.M., Donnelly-Nolan, J.M., Sherrod, D.R., 2002. North-central Oregon Cascades: exploring petrologic and tectonic intimacy in a propagating intra-arc rift. Field Guide to Geologic Processes in Cascadia. vol. 36, pp. 47–90.

Dettinger, M.P., Quade, J., 2014. Testing the Analytical Protocols and Calibration of Volcanic Glass for the Reconstruction of Hydrogen Isotopes in Paleoprecipitation. vol. 212 pp. 261–276.
Ehlers, T.A., Poulsen, C.J., 2009. Influence of Andean uplift on climate and paleoaltimetry estimates. Earth Planet. Sci. Lett. 281, 238–248.
Fan, M., Heller, P., Allen, S.D., Hough, B.G., 2014. Middle Cenozoic uplift and concomitant drying in the central Rocky Mountains and adjacent Great Plains. Geology 42, 547–550.
Fiebelkorn, R.B., Walker, G.W., MacLeod, N.S., McKee, E., Smith, J.G., 1982. Index of K-Ar Age Determinations for the State of Oregon. USGS.
Friedman, I., Smith, R.L., Long, W.D., 1966. Hydration of natural glass and formation of perlite. Geol. Soc. Am. Bull. 77, 323–328.
Friedman, I., Gleason, J., Sheppard, R.A., Gude, A.J., 1993a. Deuterium fractionation as water diffuses into silicic volcanic ash. 321–323.
Friedman, I., Gleason, J., Warden, A., 1993b. Ancient Climate From Deuterium Content of Water in Volcanic Glass. pp. 309–319.
Galewsky, J., 2009. Rain shadow development during the growth of mountain ranges: an atmospheric dynamics perspective. J. Geophys. Res. 114.
Garzione, C.N., Quade, J., DeCelles, P.G., English, N.B., 2000. Predicting paleoelevation of Tibet and the Himalaya from d18O vs. altitude gradients in meteoric water across the Nepal Himalaya. Earth Planet. Sci. Lett. 183, 215–229.
Gat, J., 1996. Oxygen and hydrogen isotopes in the hydrologic cycle. Annu. Rev. Earth Planet. Sci. 24, 225–262.
Giachetti, T., Gonnermann, H., 2013. Water in volcanic pyroclast: rehydration or incomplete degassing? Earth Planet. Sci. Lett. 369, 317–332.
Giachetti, T., Gonnermann, H.M., Gardner, J.E., Shea, T., Gouldstone, A., 2015. Discriminating secondary from magmatic water in rhyolitic matrix-glass of volcanic pyroclasts using thermogravimetric analysis. Geochim. Cosmochim. Acta 148, 457–476.
Gin, S., Guittonneau, C., Godon, N., Neff, D., Rebiscoul, D., Cabié, M., Mostefaoui, S., 2011. Nuclear glass durability: new insight into alteration layer properties. J. Phys. Chem. C 115, 18696–18706.
Gin, S., Jollivet, P., Fournier, M., Angeli, F., Frugier, P., Charpentier, T., 2015. Origin and consequences of silicate glass passivation by surface layers. Nat. Commun. 6, 6360.
Gin, S., Collin, M., Jollivet, P., Fournier, M., Minet, Y., Dupuy, L., Mahadevan, T., Kerisit, S., Du, J., 2018. Dynamics of self-reorganization explains passivation of silicate glasses. Nat. Commun. 9, 2169.
Gonfiantini, R., 1986. Environmental isotopes in lake studies. Handbook of Environmental Isotope Geochemistry. vol. 2, pp. 113–168.
Greene, R.C., 1973. Petrology of the welded tuff of Devine Canyon, southeastern Oregon. US Govt. Print. Off.
Guffanti, M., Weaver, C.S., 1988. Distribution of late Cenozoic volcanic vents in the Cascade Range: volcanic arc segmentation and regional tectonic considerations. J. Geophys. Res. Solid Earth 93, 6513–6529.
Harford, C.L., Sparks, R.S.J., 2001. Recent remobilisation of shallow-level intrusions on Montserrat revealed by hydrogen isotope composition of amphiboles. Earth Planet. Sci. Lett. 185, 285–297.
Hellmann, R., Cotte, S., Cadel, E., Malladi, S., Karlsson, L.S., Lozano-Perez, S., Cabié, M., Seyeux, A., 2015. Nanometre-scale evidence for interfacial dissolution–reprecipitation control of silicate glass corrosion. Nat. Mater. 14, 307.
Ingebritsen, S.E., Mariner, R., 2010. Hydrothermal heat discharge in the Cascade Range, northwestern United States. J. Volcanol. Geotherm. Res. 196, 208–218.
Jordan, B.T., Grunder, A.L., Duncan, R.A., Deino, A.L., 2004. Geochronology of age-progressive volcanism of the Oregon High Lava Plains: Implications for the plume interpretation of Yellowstone. J. Geophys. Res. Solid Earth 109.
Kar, N., Garzione, C.N., Jaramillo, C., Shanahan, T., Carlotto, V., Pullen, A., Moreno, F., Anderson, V., Moreno, E., Eiler, J., 2016. Rapid regional surface uplift of the northern Altiplano plateau revealed by multiproxy paleoclimate reconstruction. Earth Planet. Sci. Lett. 447, 33–47.
Kent, A.J., 2008. Melt inclusions in basaltic and related volcanic rocks. Rev. Mineral. Geochem. 69, 273–331.
Kent-Corson, M.L., Ritts, B.D., Zhuang, G., Bovet, P.M., Graham, S.A., Page Chamberlain, C., 2009. Stable isotopic constraints on the tectonic, topographic, and climatic evolution of the northern margin of the Tibetan Plateau. Earth Planet. Sci. Lett. 282, 158–166.
Kleinhans, L.C., Balcells-Baldwin, E.A., Jones, R.E., 1984. A Paleogeographic Reinterpretation of Some Middle Cretaceous Units, North-central Oregon: Evidence for a Submarine Turbidite System.
Kohn, M.J., Cerling, T.E., 2002. Stable Isotope Compositions of Biological Apatite. Phosphates; Geochemical, Geobiological, and Materials Importance. vol. 48 pp. 455–488.
Kohn, M.J., Law, J.M., 2006. Stable isotope chemistry of fossil bone as a new paleoclimate indicator. Geochim. Cosmochim. Acta 70, 931–946.
Kohn, M.J., Miselis, J.L., Fremd, T.J., 2002. Oxygen isotope evidence for progressive uplift of the Cascade Range, Oregon. Earth Planet. Sci. Lett. 204, 151–165.
Kurita, N., Yamada, H., 2008. The role of local moisture recycling evaluated using stable isotope data from over the middle of the Tibetan Plateau during the monsoon season. J. Hydrometeorol. 9, 760–775.
Kyser, T.K., O'Neil, J.R., 1984. Hydrogen isotope systematics of submarine basalts. Geochim. Cosmochim. Acta 48, 2123–2133.
Laib, A.C., 2016. Pre-Eruptive Timescales and Processes of Large Shallow Magma Systems Revealed by Compositional Variability in Silicic Ignimbrites.
Lechler, A.R., Galewsky, J., 2013. Refining paleoaltimetry reconstructions of the Sierra Nevada, California, using air parcel trajectories. Geology 41, 259–262.
Lechler, A.R., Huntington, K.W., Breecker, D.O., Sweeney, M.R., Schauer, A.J., 2018. Loess–paleosol carbonate clumped isotope record of late Pleistocene–Holocene climate change in the Palouse region, Washington State, USA. Quat. Res. 90, 331–347.
Leier, A., McQuarrie, N., Garzione, C., Eiler, J., 2013. Stable isotope evidence for multiple pulses of rapid surface uplift in the Central Andes, Bolivia. Earth Planet. Sci. Lett. 371, 49–58.
Martin, E., Bindeman, I., Balan, E., Palandri, J., Seligman, A., Villemant, B., 2017. Hydrogen isotope determination by TC/EA technique in application to volcanic glass as a window into secondary hydration. J. Volcanol. Geotherm. Res. 348, 49–61.
McCaffrey, R., King, R.W., Wells, R.E., Lancaster, M., Miller, M.M., 2016. Contemporary deformation in the Yakima fold and thrust belt estimated with GPS. Geophys. J. Int. 207, 1–11.
McClaughry, J.D., Niewendorp, C.A., Herinckx, H.H., and Duda, C.J.M., unpublished, Geologic map of the Wolf Run and northern part of the Friend 7.5' quadrangles, Wasco County, Oregon scale 1:24,000: Oregon Department of Geology and Mineral Industries Geological Map Series GMS. (unpublished)
Moore, G., 2008. Interpreting H2O and CO2 contents in melt inclusions: constraints from solubility experiments and modeling. Rev. Mineral. Geochem. 69, 333–362.
Mulch, A., Graham, S.A., Chamberlain, C.P., 2006. Hydrogen isotopes in Eocene river gravels and paleoelevation of the Sierra Nevada. Science 313, 87–89.
Mulch, A., Sarna-Wojcicki, A.M., Perkins, M.E., Chamberlain, C.P., 2008. A Miocene to Pleistocene climate and elevation record of the Sierra Nevada (California). Proc. Natl. Acad. Sci. U. S. A. 105, 6819–6824.
Niem, A.R., Niem, W.A., Martin, M.W., 1985. Oil and Gas Investigation of the Astoria Basin, Clatsop and Northernmost Tillamook Counties, Northwest Oregon. Department of Geology and Mineral Industries, State of Oregon.
Niem, W., Niem, A., Snavely Jr., P., 1992. Early and Mid-Tertiary oceanic realm and continental margin—Western Washington-Oregon coastal sequence. The Cordilleran Orogen: Conterminous US: Boulder, Colorado, Geological Society of America, The Geology of North America 3, 265–270.
Nolan, G.S., Bindeman, I.N., 2013. Experimental investigation of rates and mechanisms of isotope exchange (O, H) between volcanic ash and isotopically-labeled water. Geochim. Cosmochim. Acta 111, 5–27.
Peterson, N., Groh, E., 1970. Geologic tour of Cove Palisades State Park near Madras, Oregon. The Ore Bin 32, 141–168.
Pingel, H., Alonso, R.N., Mulch, A., Rohrmann, A., Sudo, M., Strecker, M.R., 2014. Pliocene orographic barrier uplift in the southern Central Andes. Geology 42, 691–694.
Pitcher, B.W., Kent, A.J., Grunder, A.L., Duncan, R.A., 2017. Frequency and volumes of ignimbrite eruptions following the Late Neogene initiation of the Central Oregon High Cascades. J. Volcanol. Geotherm. Res. 339, 1–22.
Poage, M.A., Chamberlain, C.P., 2001. Empirical relationships between elevation and the stable isotope composition of precipitation and surface waters; considerations for studies of paleoelevation change. Am. J. Sci. 301, 1–15.
Priest, G.R., 1990. Volcanic and tectonic evolution of the Cascade volcanic arc, central Oregon. J. Geophys. Res. Solid Earth 95, 19583–19599.
Reidel, S.P., Camp, V.E., Tolan, T.L., Martin, B.S., 2013. The Columbia River flood basalt province: stratigraphy, areal extent, volume, and physical volcanology. The Columbia River flood basalt province. Geological Society of America Special Paper. vol. 497, pp. 1–43.
Reiners, P.W., Ehlers, T.A., Garver, J.I., Mitchell, S.G., Montgomery, D.R., Vance, J.A., Nicolescu, S., 2002. Late Miocene exhumation and uplift of the Washington Cascade Range. Geology 30, 767–770.
Retallack, G., 1991. A field guide to mid-tertiary paleosols and paleoclimatic changes in the high desert of central Oregon part 1. Or. Geol. 53, 51–59.
Retallack, G.J., 2004. Late Oligocene bunch grassland and early Miocene sod grassland paleosols from central Oregon, USA. Palaeogeogr. Palaeoclimatol. Palaeoecol. 207, 203–237.
Retallack, G.J., Tanaka, S., Tate, T., 2002. Late Miocene advent of tall grassland paleosols in Oregon. Palaeogeogr. Palaeoclimatol. Palaeoecol. 183, 329–354.
Retallack, G.J., Orr, W.N., Prothero, D.R., Duncan, R.A., Kester, P.R., Ambers, C.P., 2004a. Eocene-Oligocene extinction and paleoclimatic change near Eugene, Oregon. Geol. Soc. Am. Bull. 116, 817.
Retallack, G.J., Wynn, J.G., Fremd, T.J., 2004b. Glacial-interglacial–scale paleoclimatic change without large ice sheets in the Oligocene of central Oregon. Geology 32, 297–300.
Robinson, P.T., Brem, G.F., McKee, E.H., 1984. John Day Formation of Oregon: a distal record of early Cascade volcanism. Geology 12, 229–232.
Robinson, P.T., Walker, G.W., McKee, E.H., 1990. Eocene (?), Oligocene, and lower Miocene rocks of the Blue Mountains region. Geology of the Blue Mountains Region of Oregon, Idaho, and Washington: Cenozoic Geology of the Blue Mountains Region: US Geological Survey, pp. 29–61 Professional Paper 1437.
Roe, G.H., 2005. Orographic precipitation. Annu. Rev. Earth Planet. Sci. 33, 645–671.
Rohrmann, A., Sachse, D., Mulch, A., Pingel, H., Tofelde, S., Alonso, R.N., Strecker, M.R., 2016. Miocene orographic uplift forces rapid hydrological change in the southern central Andes. Sci. Rep. 6, 35678.
Ross, C.S., Smith, R.L., 1955. Water and other volatiles in volcanic glasses. Am. Mineral. 40, 1071–1089.
Rowley, D.B., Garzione, C.N., 2007. Stable isotope-based paleoaltimetry. Annu. Rev. Earth Planet. Sci. 35, 463–508.
Rozanski, K., Araguas-Araguas, L., Gonfiantini, R., 1993. Isotopic patterns in modern global precipitation. Climate change in continental isotopic records 78, 1–36.
Sanyal, P., Bhattacharya, S.K., Prasad, M., 2005. Chemical diagenesis of Siwalik sandstone: isotopic and mineralogical proxies from Surai Khola section, Nepal. Sediment. Geol. 180, 57–74.
Sarna-Wojcicki, A.M., 1984. Chemical Analyses, Correlations, and Ages of Upper Pliocene and Pleistocene Ash Layers of East-central and Southern California.
Savoie, B.Y., 2013. Arsenic Mobility and Compositional Variability in High-Silica Ash Flow Tuffs: Portland State University.
Saylor, J.E., Horton, B.K., 2014. Nonuniform surface uplift of the Andean plateau revealed by deuterium isotopes in Miocene volcanic glass from southern Peru. Earth Planet. Sci. Lett. 387, 120–131.
Saylor, J.E., Mora, A., Horton, B.K., Nie, J., 2009. Controls on the isotopic composition of surface water and precipitation in the Northern Andes, Colombian Eastern Cordillera. Geochim. Cosmochim. Acta 73, 6999–7018.

Schmandt, B., Humphreys, E., 2011. Seismically imaged relict slab from the 55 Ma Siletzia accretion to the northwest United States. Geology 39, 175–178.
Seligman, A.N., Bindeman, I.N., Watkins, J.M., Ross, A.M., 2016. Water in volcanic glass: from volcanic degassing to secondary hydration. Geochim. Cosmochim. Acta 191, 216–238.
Sheppard, R., Gude, J., 1968. Distribution and Genesis of anthigenic silicate minerals in tuff of Pleistocene Lake Tecopa. California Professional Paper 597. US Geological Survey, Inyo County.
Sherrod, D.R., Smith, J.G., 2000. Geologic Map of Upper Eocene to Holocene Volcanic and Related Rocks of the Cascade Range, Oregon. US Geological Survey Washington, DC.
Smith, G.A., 1985. Stratigraphy, sedimentology, and petrology of Neogene rocks in the Deschutes Basin, central Oregon: A record of continental-margin volcanism and its influence on fluvial sedimentation in an arc-adjacent basin.
Smith, G.A., Snee, L.W., Taylor, E.M., 1987. Stratigraphic, sedimentologic, and petrologic record of late Miocene subsidence of the central Oregon High Cascades. Geology 15, 389–392.
Smith, J.G., 1993. Geologic Map of Upper Eocene to Holocene Volcanic and Related Rocks in the Cascade Range, Washington. Geological Survey, US.
Smith, M.E., Cassel, E.J., Jicha, B.R., Singer, B.S., Canada, A.S., 2017. Hinterland drainage closure and lake formation in response to middle Eocene Farallon slab removal, Nevada, U.S.A. Earth Planet. Sci. Lett. 479, 156–169.
Smith, R.B., Barstad, I., Bonneau, L., 2005. Orographic precipitation and Oregon's climate transition. J. Atmos. Sci. 62, 177–191.
Smith, R.L., 1960a. Ash flows. Geol. Soc. Am. Bull. 71, 795–841.
Smith, R.L., 1960b. Zones and Zonal Variations in Welded Ash Flows.
Snavely Jr., P.D., Wells, R.E., 1996. Cenozoic evolution of the continental margin of Oregon and Washington. Assessing Earthquake Hazards and Reducing Risk in the Pacific Northwest. vol. 1, pp. 161–182.
Streck, M.J., Grunder, A.L., 1995. Crystallization and welding variations in a widespread ignimbrite sheet; the Rattlesnake Tuff, eastern Oregon, USA. Bull. Volcanol. 57, 151–169.
Streck, M.J., Grunder, A.L., Johnson, J.A., 1999. Field guide to the Rattlesnake Tuff and high Lava plains near Burns, Oregon.
Streck, M., Ferns, M., Haller, K., Wood, S., 2004. The Rattlesnake Tuff and other Miocene silicic volcanism in eastern Oregon. Geological Field Trips in southern Idaho, eastern Oregon, and northern Nevada (2004-1222).
Takeuchi, A., Larson, P.B., 2005. Oxygen isotope evidence for the late Cenozoic development of an orographic rain shadow in eastern Washington, USA. Geology 33, 313.
Takeuchi, A., Hren, M.T., Smith, S.V., Chamberlain, C.P., Larson, P.B., 2010. Pedogenic carbonate carbon isotopic constraints on paleoprecipitation: evolution of desert in the Pacific Northwest, USA, in response to topographic development of the Cascade Range. Chem. Geol. 277, 323–335.
Talbot, M., 1990. A review of the palaeohydrological interpretation of carbon and oxygen isotopic ratios in primary lacustrine carbonates. Chem. Geol. Isot. Geosci. 80, 261–279.
Taylor, E.M., 1990. Volcanic history and tectonic development of the central High Cascade Range, Oregon. J. Geophys. Res. Solid Earth 95, 19611–19622.
Techer, I., Lancelot, J., Clauer, N., Liotard, J.M., Advocat, T., 2001. Alteration of a basaltic glass in an argillaceous medium:: the Salagou dike of the Lodève Permian Basin (France). Analogy with an underground nuclear waste repository. Geochim. Cosmochim. Acta 65, 1071–1086.
Valle, N., Verney-Carron, A., Sterpenich, J.m., Libourel, G., Deloule, E., Jollivet, P., 2010. Elemental and isotopic (29Si and 18O) tracing of glass alteration mechanisms. Geochim. Cosmochim. Acta 74, 3412–3431.
Vance, J., 1988. New fission track and K-Ar ages from the Clarno formation, Challis age volcanic rocks in north central Oregon. Geological Society of America, Rocky Mountain Section, Abstracts With Programs, p. 473.
Verplanck, E.P., Duncan, R.A., 1987. Temporal variations in plate convergence and eruption rates in the Western Cascades, Oregon. Tectonics 6, 197–209.
Wang, Y., Cheng, H., Edwards, R.L., Kong, X., Shao, X., Chen, S., Wu, J., Jiang, X., Wang, X., An, Z., 2008. Millennial-and orbital-scale changes in the East Asian monsoon over the past 224,000 years. Nature 451, 1090–1093.
Wells, R., Bukry, D., Friedman, R., Pyle, D., Duncan, R., Haeussler, P., Wooden, J., 2014. Geologic history of Siletzia, a large igneous province in the Oregon and Washington Coast Range: correlation to the geomagnetic polarity time scale and implications for a long-lived Yellowstone hotspot. Geosphere 10, 692–719.
Wells, R.E., Heller, P.L., 1988. The relative contribution of accretion, shear, and extension to Cenozoic tectonic rotation in the Pacific Northwest. Geol. Soc. Am. Bull. 100, 325–338.
Wells, R.E., McCaffrey, R., 2013. Steady rotation of the Cascade arc. Geology 41, 1027–1030.
Whiteman, C.D., 2000. Mountain Meteorology: Fundamentals and Applications. Oxford University Press.
Zachos, J., Pagani, M., Sloan, L., Thomas, E., Billups, K., 2001. Trends, rhythms, and aberrations in global climate 65 Ma to present. Science 292, 686–693.
Zachos, J.C., Stott, L.D., Lohmann, K.C., 1994. Evolution of early Cenozoic marine temperatures. Paleoceanography 9, 353–387.
Zhou, Q., Liu, L., 2019. Topographic evolution of the western United States since the early Miocene. Earth Planet. Sci. Lett. 514, 1–12.